

# DNA methylation in peripheral blood leukocytes in late onset Alzheimer's disease

Journal of Alzheimer's  
Disease Reports  
Volume 9: 1–16  
© The Author(s) 2025  
Article reuse guidelines:  
sagepub.com/journals-permissions  
DOI: 10.1177/25424823251341176  
journals.sagepub.com/home/alr



Tatiana Chacón<sup>1,2</sup> and Hernán G Hernández<sup>1</sup>

## Abstract

**Background:** Chronic systemic inflammation is implicated in Alzheimer's disease (AD) pathogenesis and has measurable effects on blood cells. There is increasing interest in non-invasive diagnostic tools that use blood-based biomarkers for AD, such as DNA methylation. Notably, DNA methylation changes in blood are also linked to systemic inflammation. The evaluation of DNA methylation profiles in peripheral blood leukocytes as potential biomarkers for AD is promising.

**Objective:** To determine DNA methylation patterns in blood for AD, and to explore specific blood CpG sites that act as surrogates for brain-tissue methylation.

**Methods:** DNA methylation data from peripheral blood leukocytes of AD patients and controls were obtained from the Gene Expression Omnibus (GSE59685 and GSE53740). Differential methylation analysis was performed for individual CpGs Differentially methylated positions (DMPs) and regions with multiple probes (DMRs) and the intersection analysis of DMPs and DMRs was conducted. Functional enrichment analysis highlights relevant biological processes. Furthermore, previously validated specific CpGs used as surrogate of brain tissue were explored.

**Results:** DNA methylation patterns included *BTBD3*, *PGPEPIL*, *DUSP29*, and *MIB2* top genes ordered by statistical significance were found in the intersection of DMP and DMR. Differential methylation analyses revealed differentially methylated genes including *HOXA-AS3*, *HOXA6*, *CACNA1A*, *KMT5A*, *MIDEAS*, *FAM234A*, and *KATNBLIP6*. Gene enrichment analysis showed immune processes and intracellular signaling disruptions. Surrogate genes from brain found differentially methylated were *PCDHGB1-3* and *PCDHGA1-6*.

**Conclusions:** This study identified DNA methylation patterns in peripheral blood leukocytes as potential biomarkers for AD. These findings offer insights into epigenetic mechanisms associated with systemic peripheral inflammation in AD.

## Keywords

Alzheimer's disease, biomarkers, dementia, DNA methylation, epigenetics

Received: 12 July 2024; accepted: 16 April 2025

## Introduction

Alzheimer's disease (AD) is the most common form of dementia and is characterized by a progressive decline in cognitive function. This neurodegenerative disorder particularly impairs memory and has a profound effect on the quality of life.<sup>1,2</sup> A persistent chronic systemic proinflammatory component is related to AD evidenced by the detection of alterations in blood cells and plasma.<sup>3–5</sup>

Several lines of evidence indicate that diagnosis of AD could be simplified by noninvasive and low-cost methods, such as the detection of biomarkers in blood.<sup>6–8</sup> The main epigenetic mechanisms include post-transcriptional modification of histones and DNA methylation, regulated by different pathways, which are coupled with each other.<sup>9</sup> DNA

methylation is an inheritable epigenetic modification through cellular mitosis that regulates gene expression, with no changes in genetic sequence. Blood DNA methylation has emerged as significant in a range of diseases, especially those affecting specific target organs like degenerative conditions. Therefore, this approach may

<sup>1</sup>Dentistry Faculty, Universidad Santo Tomas, Bucaramanga, Colombia

<sup>2</sup>Health Faculty, Universidad Autónoma de Manizales, Antigua Estación del Ferrocarril, Manizales, Colombia

## Corresponding author:

Hernán Guillermo Hernández, Dentistry Faculty, Universidad Santo Tomas, Carrera 27# 180 - 395, Bucaramanga, Santander, Colombia.  
Email: hernan.hernandez.md@gmail.com



Creative Commons Non Commercial CC BY-NC: This article is distributed under the terms of the Creative Commons Attribution-NonCommercial 4.0 License (<https://creativecommons.org/licenses/by-nc/4.0/>) which permits non-commercial use, reproduction and distribution of the work without further permission provided the original work is attributed as specified on the SAGE and Open Access page (<https://us.sagepub.com/en-us/nam/open-access-at-sage>).

**Table 1.** Demographic characteristics of the included subjects by group.

Variable\Group	AD (n = 52)	Control (n = 111)	p
Age, mean (SD)	82.57 (8.50)	70.72 (10.53)	0.00001 <sup>‡</sup>
Sex			
Female	35	66	
Male	17	45	0.43016 <sup>‡</sup>

SD: standard deviation; <sup>‡</sup>Student's t-test, <sup>‡</sup>Chi -square test.

contribute with insights of the pathophysiology of the epigenetic phenomena which is associated with systemic inflammation in AD. A line of studies have investigated peripheral blood DNA methylation of AD patients using different approaches, including arrays;<sup>10</sup> interestingly, the use blood DNA as a surrogate of brain tissue to analyze changes in CpG methylation level has been reported in different contexts.<sup>11–13</sup> Thus, the use of epigenetic biomarkers in blood is a valid approach to systemic physiopathology of this kind of neurodegenerative disease.<sup>11,12,14</sup>

Recent genome-wide methylation studies show that DNA methylation signatures in blood can serve as biomarkers for AD. For instance, multiple groups have reported differential methylation in blood between AD patients and controls.<sup>15</sup> Our study builds on this framework with a novel approach: we incorporate an analysis of surrogate CpG sites – CpG loci in blood that correlate strongly with brain methylation patterns.<sup>16</sup> This approach offers a new perspective on how peripheral methylation changes might mirror central nervous system epigenetic changes. By performing standard differential methylation analyses and then specifically examining these brain-surrogate CpGs, we aim to provide a more comprehensive view of AD-associated epigenetic alterations and to contribute to the future development of non-invasive biomarkers.

Inflammation is an important factor in diseases such as diabetes, atherosclerosis, rheumatoid arthritis, and neurodegenerative disorders.<sup>17,18</sup> For example, increased levels of proinflammatory cytokines such as TNF- $\alpha$ , IL-6, IL-1, IL-8, and IFN- $\gamma$  have been reported in the serum and brain tissue of AD patients compared to healthy controls.<sup>19,20</sup> Pathological processes in cells and tissues trigger changes in gene expression and regulation in blood cells, which allow gene expression/epigenetic profiling for diagnostic purposes.<sup>21</sup> It is noteworthy that epigenetic mechanisms have been shown to determine the susceptibility, modulation, final effects of the inflammatory response and, recently, the response to treatment in other inflammatory diseases.<sup>22,23</sup>

In this context, it is proposed to determine the DNA methylation profiles in peripheral blood leukocytes as candidate biomarkers for AD, aiming to contribute insights into epigenetic phenomena potentially associated with peripheral systemic inflammation in AD and using blood DNA as a surrogate of brain tissue.<sup>24,25</sup>

**Table 2.** Demographic characteristics of the included profiles by primary dataset.

Dataset\Variables	Age mean $\pm$ SD	Sex (n)
GSE59685 (London cohort)	83.23 $\pm$ 6.97	Male = 45 Female = 61
GSE53740 (Memory and Aging Center)	69.82 $\pm$ 10.45	Male = 17 Female = 40

All epigenomic profiles were annotated as “Caucasian,” “White,” or part of the London Cohort to attempt to maintain a uniform ethnic origin.

This work tried to elucidate the relevance of these profiles, with a novel approach that includes CpGs highly correlated between blood and brain with strong statistical significance, considered as surrogate CpGs by Braun et al.<sup>16</sup> In this context, it is proposed to determine whether the DNA methylation profiles in peripheral blood leukocytes could serve as candidate biomarkers for AD, and to explore the potential contribution of surrogate CpGs to these profiles. These efforts seek to provide insights into epigenetic phenomena potentially associated with peripheral systemic inflammation in AD and its relationship with brain tissue.

## Methods

### Population

Data included DNA methylation profiles from peripheral blood leukocytes from subjects over 60 years with phenotypic annotations that indicate AD in intermediate to advanced stage compared to controls. GSE59685 and GSE53740 datasets available in Gene Expression Omnibus (GEO) were used. Considering only peripheral blood samples of interest, a total of 288 samples were available. Samples were excluded if they were labeled as “excluded” in the primary dataset or if they had missing values in the sex variable. To enhance homogeneity, only samples with epigenomic profiles annotated as “Caucasian,” “White,” or part of the London Cohort were selected to ensure a uniform ethnic origin. From those, 223 samples were evaluated for quality control with p detection values. Finally, 163 samples (mean  $\pm$  SD: 74.51  $\pm$  11.35) were selected for analysis; 52 AD subjects (67.3% female) and 111 control subjects (60.0% female) were analyzed (Table 1).

Two independent cohorts were included in this study: the London cohort<sup>26,27</sup> and the UCSF Memory and Aging Center cohort.<sup>28</sup> These cohorts had been previously analyzed for other research questions; however, in the present investigation, the DNA methylation data were obtained from the GEO (accessions GSE59685 for London and GSE53740 for UCSF). The original studies secured appropriate informed consent and ethical approvals.<sup>26–28</sup>

Table 2 summarizes the participants' demographics. In the London cohort, the mean age was 83.23  $\pm$  6.97 years

(45 males, 61 females), whereas in the Memory and Aging Center cohort the mean age was  $69.82 \pm 10.45$  years (17 males, 40 females). Only samples annotated as 'Caucasian' or 'White' (or belonging to the London cohort) were selected to maintain a uniform ethnic background across samples.

### Data importing and preprocessing

DNA methylation epigenomic data processed by *Illumina Infinium 450k Human DNA methylation Beadchip* were obtained from public *GENE Expression Omnibus* repositories.<sup>29</sup> Analyses were carried out using R/Bioconductor environment. DNA methylation profiles were imported with GetGEO function from GEOquery package.<sup>30</sup> To curate the database, a thorough review of the data was conducted, employing both automated and manual processes. Probes directed to CpGs in sex chromosomes were excluded to increase sample comparability, as the dataset included both sexes, potentially leading to bias driven by sex-specific DNA methylation in the X and Y chromosomes.<sup>31</sup> Raw methylation data Beta values were preprocessed by BMIQ (Beta Mixture Quantile dilation) normalization strategy combined with *ComBat* algorithm, which employs an empirical Bayes framework to remove systematic technical variation (Batch Correction). This combination has proven benefits in eliminating the batch effect of samples present in different technical settings.<sup>32</sup> Given the implementation of BMIQ normalization, beta values were used in the differential analysis. DNA methylation epigenomic data processed by *Illumina Infinium 450k Human DNA methylation Beadchip* were obtained from public *GENE Expression Omnibus* repositories.<sup>29</sup> Analyses were carried out using R/Bioconductor environment. DNA methylation profiles were imported with GetGEO function from GEOquery package.<sup>30</sup> To curate the database, a thorough review of the data was conducted, employing both automated and manual processes. Probes directed to CpGs in sex chromosomes were excluded to increase sample comparability, as the dataset included both sexes, potentially leading to bias driven by sex-specific DNA methylation in the X and Y chromosomes.<sup>31</sup> Raw methylation data Beta values were preprocessed by BMIQ (Beta Mixture Quantile dilation) normalization strategy combined with *ComBat*. This combination has proven benefits in eliminating the batch effect of samples present in different technical settings.<sup>32</sup> Given the implementation of BMIQ normalization, beta values were used in the differential analysis.

For quality control, *p* detection value filter was set at  $>1 \times 10^{-12}$ ; this threshold was selected, considering that values near to zero prevent spurious results.<sup>33,34</sup> Additionally, sex chromosome filtering and filters for single nucleotide polymorphisms (SNPs) and CH sites were applied through *minfi* R package *dropMethylationLoci* function as previously described.<sup>35</sup>

### Analysis of differentially methylated positions (DMPs)

*Limma* package was used to determine differential methylation between AD and Controls. DMP were determined through robust regression (using iterative least squares method) to assess methylation contrasts between each group. In addition, an estimation of the cell types was made using the function *estimateCellCounts* of *minfi*. The model included age, sex and cell distribution of neutrophil, monocytes, CD8+, CD4+, Natural Killer, and B lymphocytes. The significance threshold was set at  $p < 0.05$  after Bonferroni correction. A Delta of Beta filter (percentage of methylation) was set to 0.06.

### Analysis of differentially methylated regions (DMRs)

DMR analysis allows to determine regions where consecutive differentially methylated CpGs are present. DMRs were analyzed using *DMRcate* package, which extracts the regions with greatest differential methylation and regions with variable methylation from *Illumina* DNA methylomes. In addition, a Delta of Beta filter ( $>0.05$ ) was used by adding the parameter *DeltaBetaCutoffNetMean* as previously reported.<sup>31,35</sup> *p* values were adjusted by control for false discovery rate (FDR), using the Benjamini-Hochberg method ( $p < 0.05$ ). In this study, DMRs were identified using *DMRcate*, defining them as regions where consecutive probes, separated by no more than 200 nucleotides, exhibited differential methylation in the same direction.

### DMP-DMR intersection analysis

To increase biological significance to the interpretation of the results, an intersection analysis between DMP and DMR results was achieved by *GRanges* package detecting differentially methylated intersections to determine the most relevant candidate genes. In physical terms, these intersections correspond to exact matches in genomic coordinates between DMPs and DMRs.

### Identification of differentially methylated genes and analysis of functional enrichment

Assignment of genes to methylated probes was found by searching 2000 bp (upstream or downstream) from Transcription Start Sites (TSSs) as previously reported.<sup>35</sup> Functional enrichment analysis was performed by *FatiGO* functional process of *Babelomics* software, which allowed to determine the pathways/ontologies found significantly overrepresented in the differentially methylated genes.<sup>36</sup>

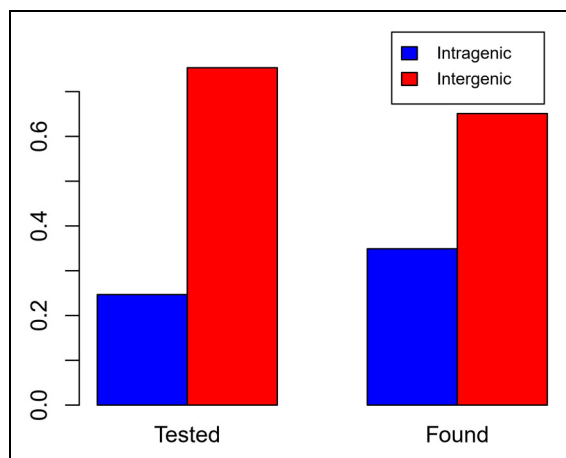


**Figure 1.** The bar chart shows the proportion of intragenic (blue) and intergenic (red) CpGs among all tested probes ("Tested") and those found to be differentially methylated in AD ("Found"). Among the CpGs analyzed, 24.68% were intragenic and in the differentially methylated subset were 34.91%.

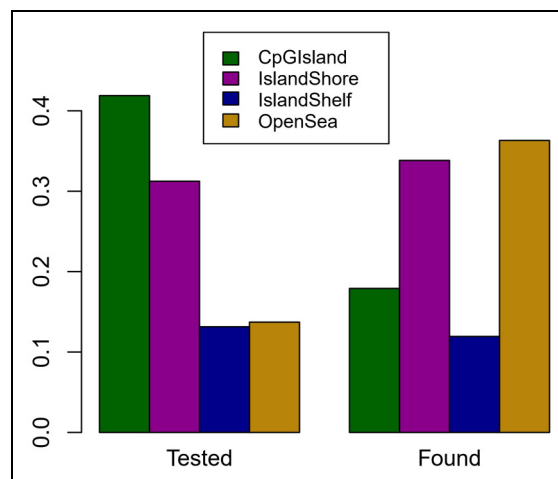


**Figure 2.** The bar chart shows the comparative distribution of CpG island-associated regions (CpGIsland, IslandShore, IslandShelf, OpenSea) in tested vs. differentially methylated CpG sites in AD.

### Identification of differential methylation in brain surrogated positions

To explore differential methylation positions in blood as surrogates of brain tissue, an additional analysis was performed in 989 surrogated CpGs for 450K, previously reported as representative of brain tissue due to a high correlation between brain and blood tissues.<sup>16</sup>

## Results

Sex distribution of AD subjects was comparable to controls (chi-square  $p$  value: 0.43). The age of AD subjects differed from controls (mean  $\pm$  SD:  $82.6 \pm 8.5$  versus  $70.7 \pm 10.5$ , t-test  $p$  value  $< 0.001$ ); the statistical model included age to control such difference. Distribution of cell types determined by estimateCellCounts function are shown in Supplemental Table 1.

From a number of 484577 probes in the array, 27444 were excluded due to  $p$  detection value exceeding the threshold, leaving 457133 probes. After filtering sex chromosome, 447115 probes remained. Finally, employing *dropmethylationloci* function for SNP and CH filtering, 444850 probes were selected to be included in the analysis (Supplemental Figure 1).

DMP analysis resulted in 201 differentially methylated probes; 114 differentially hypermethylated and 87 differentially hypomethylated probes. A post-hoc power calculation confirmed that our sample size ( $n = 163$ ) provided  $\sim 86\%$  power (at  $\alpha = 0.05$ ) to detect effect sizes corresponding to at least five significantly differentially methylated genes, which is in line with the number of loci we observed. From the differentially hypermethylated probes, 89 were assigned to one or more genes as one gene may have

more than one probe assigned. Among the CpGs analyzed, 24.68% were located within gene regions, 75.32% intergenic; in contrast, the proportion of intragenic positions among the differentially methylated sites was 34.91%, 65.1% intergenic (Figure 1).

A comparative analysis of CpG site distribution across CpG islands, island shores, island shelves, and open sea was conducted for both the tested and differentially methylated CpGs in AD. Among the tested set, 41.89% were located in CpG islands, whereas only 17.91% of the differentially methylated CpGs fell into these regions. Island shores also showed a slight increase in their proportion, suggesting that the transition zones flanking CpG islands may be relevant for AD-related methylation changes. Conversely, open sea regions rose from 13.72% in the tested set to 36.32% in the differentially methylated group. A chi-square test confirmed these shifts were highly significant ( $\chi^2 \approx 103.4$ ,  $df = 3$ ,  $p < 2.2 \times 10^{-1}$ ), indicating a marked redistribution of CpGs in AD. Overall, differentially methylated CpGs appear enriched outside CpG islands, underscoring the potential significance of both island shores and non-island regions in AD-associated epigenetic alterations (Figure 2).

Of the differentially hypomethylated probes, 55 were assigned to one or more genes. Table 2 shows top differentially hypermethylated positions assigned to genes, including *HOXA-AS3/HOXA6*. Table 3 illustrates the top differentially hypomethylated positions assigned to genes including *KMT5A*. Table 4 shows the top differentially hypermethylated positions. Supplemental Table 2 contains the total DMP results.

Regions represented by three or more probes are shown due to their theoretical biological relevance in comparison to isolated CpGs. According to its relevance FAM234A

**Table 3.** Differentially hypermethylated CpGs in AD assigned to genes (top 30).

Probe Id	Chr	Gene symbol	$\Delta\beta$	t	B	Adj. p	Dir
cg18931036	chr7	<i>HOXA-AS3, HOXA6</i>	0.10	17.25	76.21	1.36E-32	Hyper
cg12581769	chr19	<i>CACNA1A</i>	0.07	12.62	47.45	4.37E-20	Hyper
cg04591034	chr5	<i>COL23A1</i>	0.16	11.05	37.51	9.09E-16	Hyper
cg00700039	chr18	<i>SMCHD1</i>	0.13	10.30	32.81	9.95E-14	Hyper
cg09813647	chr17	<i>RNF213-AS1, RNF213</i>	0.12	9.96	30.77	8.16E-13	Hyper
cg08531052	chr19	<i>PPFIA3</i>	0.07	9.82	29.83	2.01E-12	Hyper
cg17086141	chr17	<i>NPEPPS</i>	0.06	9.44	27.58	1.96E-11	Hyper
cg22496986	chr17	<i>CAMKK1</i>	0.11	9.22	26.20	7.86E-11	Hyper
cg22719308	chr1	<i>PTPN14</i>	0.07	8.23	20.37	2.77E-08	Hyper
cg25641145	chr8	<i>ANKRD46</i>	0.10	8.23	20.34	2.86E-08	Hyper
cg24196017	chr15	<i>CDAN1</i>	0.07	8.07	19.40	7.35E-08	Hyper
cg07147421	chr10	<i>FAM245A</i>	0.09	8.06	19.37	7.56E-08	Hyper
cg23047825	chr15	<i>IGF1R</i>	0.07	7.97	18.83	1.32E-07	Hyper
cg14429807	chr9	<i>VAV2</i>	0.06	7.94	18.75	1.51E-07	Hyper
cg23672278	chr1	<i>EVA1B, SH3D21</i>	0.09	7.87	18.29	2.26E-07	Hyper
cg08198187	chr12	<i>AMN1</i>	0.08	7.74	17.56	4.76E-07	Hyper
cg19151808	chr4	<i>NAP1L5, HERC3</i>	0.08	7.74	17.61	4.83E-07	Hyper
cg20805133	chr2	<i>PDCD1</i>	0.10	7.65	17.05	7.98E-07	Hyper
cg01697477	chr3	<i>RARB</i>	0.07	7.40	15.66	3.31E-06	Hyper
cg09219566	chr12	<i>PEBP1</i>	0.07	7.33	15.23	4.94E-06	Hyper
cg03301058	chr6	<i>GABRR2</i>	0.21	7.32	15.19	5.28E-06	Hyper
cg27529555	chr1	<i>KLHDC8A</i>	0.08	7.31	15.15	5.58E-06	Hyper
cg08925046	chr10	<i>PDLIM1</i>	0.08	7.24	14.78	7.96E-06	Hyper
cg05697969	chr19	<i>HCN2</i>	0.11	7.18	14.45	1.10E-05	Hyper
cg03072665	chr2	<i>BOK</i>	0.08	7.07	13.83	2.08E-05	Hyper
cg00025823	chr17	<i>CRHR1</i>	0.10	7.03	13.62	2.57E-05	Hyper
cg02704552	chr7	<i>SERPINE1</i>	0.08	6.96	13.25	3.71E-05	Hyper
cg17520027	chr1	<i>NR5A2</i>	0.07	6.95	13.16	4.08E-05	Hyper
cg23480697	chr6	<i>HLA-G, HLA-H</i>	0.10	6.94	13.13	4.18E-05	Hyper
cg26103179	chr12	<i>SRRM4</i>	0.06	6.91	12.96	4.94E-05	Hyper

Adj. p: Bonferroni adjusted p values; B: B-statistic corresponding to the log-odds that the CpG differentially methylated; Chr: chromosome; Dir: direction of differential methylation in AD; Gene symbol: official gene symbol of NIH available in <http://www.ncbi.nlm.nih.gov/gene>; Probe Id: alphanumeric codes corresponding to the Illumina probe/position; t: value of t-distribution;  $\Delta\beta$ : the net difference between beta values of control group and AD group (control —AD).

(ITFG3), KATNBLIP6, PGPEP1L, and DUSP29 (DUPD1) are the top genes found (Table 5). The total of DMR results are shown in Supplemental Table 3 considering that in some cases, even one CpG, could be representative of a region.

### Intersection of DMP and DMR

Table 6 shows the top results of regions found in the intersection analysis between DMRs and DMPs. The intersected regions with assigned genes including *BTBD3*, *PGPEP1L*, *DUSP29*, *MIB2*, and *HOXA6*, some of them previously mentioned. The total results are available in Supplemental Table 4.

The top results of methylation probes assigned to genes found on the intersection between DMPs and DMRs are shown on Table 7. These included *HOXA-AS3*, *HOXA6*, *KMT5A*, *MIDEAS*, *BCAM*, and *CACNA1A* genes. A total of 62 methylation probes assigned to genes were identified in intersection of the results of the regional analysis (Supplemental Table 5).

### Gene enrichment analysis

In AD group versus controls, the top results from the functional enrichment analysis of differentially methylated genes revealed the following terms in the InterPro functional enrichment: Immunoglobulin-like domain (IPR007110), CD80-like, immunoglobulin C2-set (IPR013162), Immunoglobulin subtype (IPR003599), Immunoglobulin V-set domain (IPR013106), Immunoglobulin subtype 2 (IPR003598), Immunoglobulin I-set (IPR013098) mainly related with immune response (Table 8). Additionally, only one term was found for Metabolic Network Recon enrichment “inositol Phosphate Metabolism”.

Regarding Gene Ontology functional terms, GO-Slim (Table 9) a reduced version of the Gene Ontology that contains a selected number of relevant nodes showed: extracellular matrix organization (GO:0030198), neurological system process (GO:0050877), autophagy (GO:0006914); mRNA processing (GO:0006397), translation (GO:0006412). The top results restricted to GO biological processes (Table 10) enrichment included: cell surface receptor signaling

**Table 4.** Differentially hypomethylated CpGs in AD assigned to genes (top 30).

Probe Id	Chr	Gene symbol	$\Delta\beta$	t	B	Adj. p	Dir
cg05489271	chr12	KMT5A	-0.07	-16.57	72.12	7.97E-31	Hypo
cg04285477	chr14	MIDEAS	-0.13	-16.31	70.48	4.11E-30	Hypo
cg24506130	chr2	MIR3127, CNM4	-0.06	-15.69	66.68	1.86E-28	Hypo
cg17921863	chr19	BCAM	-0.07	-13.15	50.76	1.55E-21	Hypo
cg17809780	chr3	ATG7	-0.10	-11.52	40.48	4.59E-17	Hypo
cg10649706	chr8	AGO2	-0.09	-11.25	38.76	2.58E-16	Hypo
cg25027788	chr12	VWF	-0.12	-11.09	37.76	7.03E-16	Hypo
cg13262467	chr3	LRR1Q4	-0.10	-11.02	37.38	1.06E-15	Hypo
cg13815695	chr12	TTC41P	-0.21	-10.79	35.74	5.58E-15	Hypo
cg03464200	chr7	SSPOP	-0.06	-10.58	34.55	1.76E-14	Hypo
cg05187322	chr17	CARD14	-0.15	-10.30	32.92	9.65E-14	Hypo
cg13164537	chr18	CD226	-0.09	-9.99	30.92	6.77E-13	Hypo
cg05891548	chr19	CEACAM4	-0.09	-9.96	30.76	8.07E-13	Hypo
cg07507057	chr5	PCDHA1-8 <sup>a</sup>	-0.12	-9.93	30.56	9.66E-13	Hypo
cg25256924	chr11	CORO1B, PTPRCAP	-0.09	-9.88	30.20	1.38E-12	Hypo
cg00820740	chr10	BICCI	-0.07	-9.87	30.16	1.46E-12	Hypo
cg24189340	chr11	OPCML	-0.10	-9.59	28.50	8.02E-12	Hypo
cg09564509	chr2	HDLBP	-0.09	-8.90	24.28	5.47E-10	Hypo
cg23103009	chr10	INPP5A	-0.08	-8.87	24.12	6.35E-10	Hypo
cg15287806	chr10	ZMYND11	-0.13	-8.42	21.43	9.55E-09	Hypo
cg14052044	chr19	MISP	-0.09	-8.37	21.15	1.25E-08	Hypo
cg09529323	chr19	SBK2	-0.08	-8.29	20.72	1.95E-08	Hypo
cg05940452	chr11	FOXR1	-0.16	-7.64	17.00	8.40E-07	Hypo
cg25644478	chr3	LTF	-0.08	-7.51	16.24	1.79E-06	Hypo
cg13696171	chr2	GPR35	-0.07	-7.34	15.32	4.56E-06	Hypo
cg14164099	chr15	LINC01197	-0.08	-7.19	14.51	1.05E-05	Hypo
cg16587849	chr16	TENT4B	-0.07	-7.13	14.19	1.47E-05	Hypo
cg24515368	chr1	DDAH1, LOC646626	-0.07	-7.10	13.97	1.80E-05	Hypo
cg17253835	chr13	DACH1	-0.08	-7.07	13.84	2.06E-05	Hypo
cg19961153	chr2	ALPG	-0.14	-6.89	12.88	5.50E-05	Hypo

Adj. p: Bonferroni adjusted p values; B: B-statistic corresponding to the log-odds that the CpG differentially methylated; Chr: chromosome; Dir: direction of differential methylation in AD; Gene symbol: official gene symbol of NIH available in <http://www.ncbi.nlm.nih.gov/gene>; Probe Id: alphanumeric codes corresponding to the Illumina probe/position; t: value of t-distribution;  $\Delta\beta$ : the net difference between beta values of control group and AD group (control - AD).

<sup>a</sup>Genes PCDHA 1 to PCDHA 8.

pathway (GO:0007166), intracellular signal transduction (GO:0035556), homophilic cell adhesion via plasma membrane adhesion molecules (GO:0007156), behavioral response to pain (GO:0048266), gamma-aminobutyric acid signaling pathway (GO:0007214), Notch signaling pathway (GO:0007219), regulation of ion transmembrane transport (GO:0034765), ossification (GO:0001503), skeletal system development (GO:0001501), and gene silencing by RNA (GO:0031047). No significance was found in Gene enrichment analysis for GO Molecular Function and GO cellular component.

### Brain subrogates positions

From 989 subrogated positions analyzed, one, cg09029624, was found to be differentially hypomethylated with approximately a 5% difference, corresponding to nine genes, *PCDHGA1-6* (six genes) and *PCDHGB1-3* (three genes). This result surpassed the threshold for Bonferroni correction for multiple testing (Supplemental Table 6).

## Discussion

This study performed a genome-wide DNA methylation analysis to determine profiles in peripheral blood leukocytes as candidate biomarkers in AD on intermediate to advanced stage and controls. Two complementary analyses for differential methylation, DMP and DMR, were included to increase reliability of the found patterns. DNA methylation patterns highlighted *BTBD3*, *PGPEP1L*, *DUPD1*, and *MIB2* as the top genes identified at the intersection of DMP and DMR analyses. Differential methylation analyses revealed differentially methylated genes in the top lists, including *HOXA-AS3*, *HOXA6*, *CACNA1A*, *KMT5A*, *MIDEAS*, *FAM234A*, and *KATNBL1P6*.

### BTBD3 (BTB domain containing 3)

The *BTBD3* gene is a Protein Coding that acts as a key regulator of dendritic field orientation during development of sensory cortex and directs dendrites toward active axon

**Table 5.** Top results of regions found in the DMR analysis.

Coord hg19	width	Gene	group	#p	Min p	Mean p	Mean Dbetas
chr16:303165-303192	28	FAM234A <sup>a</sup> (ITFG3)	5'UTR	3	6.35E-14	6.35E-14	-0.09
chr6:147124881-147124996	116	KATNBLIP6 <sup>a</sup>	Body, TSS200	6	9.23E-09	2.63E-08	-0.07
chr15:99548859-99549047	189	PGPEPIL <sup>a</sup>	5'UTR, 1stExon, TSS200	4	6.28E-08	9.05E-07	0.06
chr10:76803669-76803925	257	DUSP29 <sup>a</sup> (DUPD1)	Body	3	9.40E-08	1.73E-03	0.06
chr17:37123638-37123949	312	FBXO47	1stExon, 5'UTR, TSS200, TSS1500	9	1.90E-07	8.32E-06	0.08
chr1:248100183-248100614	432	OR2L13	TSS1500, TSS200, 1stExon, 5'UTR	10	2.39E-07	1.92E-03	0.09
chr10:3824387-3824687	301	KLF6	Body	4	4.36E-07	6.52E-05	0.07
chr1:1564920-1565027	108	MIB2	Body	3	5.63E-07	2.86E-05	-0.07
chr7:5111875-5112067	193	LOC389458	Body	3	1.46E-06	4.29E-04	0.06
chr5:110062343-110062473	131	TMEM232	1stExon, 5'UTR, TSS200	5	1.55E-06	2.20E-06	0.07
chr7:16505409-16505664	256	SOSTDC1	1stExon, 5'UTR, TSS200	5	2.96E-06	2.41E-04	-0.06
chr1:1564422-1564482	61	MIB2	Body	3	4.30E-06	6.75E-06	-0.06
chr19:49077983-49078119	137	SULT2B1	Body, TSS1500	3	4.39E-06	5.06E-05	-0.07
chr6:29911366-29911558	193	HLA-A	Body	5	1.59E-05	4.02E-03	0.06
chr19:36485282-36485360	79	SDHAF1	TSS1500	3	1.82E-05	2.64E-05	0.07
chr10:129797760-129797840	81	PTPRE	5'UTR	3	2.02E-05	2.14E-05	-0.08
chr4:6344361-6344484	124	PPP2R2C	Body	3	2.69E-05	4.37E-05	0.07
chr9:4662858-4663107	250	C9orf68, PPAPDC2	Body, 1stExon	3	3.31E-05	6.25E-04	0.07
chr6:37616410-37616803	394	MDGA1	Body	4	5.99E-05	6.77E-03	-0.07
chr17:13506186-13506284	99	HS3ST3A1	TSS1500	3	9.35E-05	1.16E-04	0.07
chr8:11141365-11141424	60	MTMR9	TSS1500	3	1.47E-04	2.12E-04	0.06
chr6:32551888-32552106	219	HLA-DRB1	Body	8	1.72E-04	3.79E-04	0.07
chr11:6292311-6292615	305	CCKBR	Body	4	2.04E-04	1.06E-02	0.07
chr3:44802549-44802604	56	KIF15, KIAA1143	TSS1500, Body	3	3.47E-04	4.31E-04	0.06
chr6:37617864-37618123	260	MDGA1	Body	4	3.95E-04	2.01E-03	-0.08
chr1:146649635-146649851	217	PDIA3P	Body	4	7.98E-04	7.17E-03	0.07
chr10:131669406-131669630	225	EBF3	Body	3	1.56E-03	3.89E-03	0.11
chr15:101084507-101084565	59	LASS3	5'UTR	3	3.58E-03	5.22E-03	-0.06
chr17:4487099-4487125	27	SMTNL2	TSS200, TSS1500	4	3.70E-03	3.74E-03	0.07
chr19:12876846-12877000	155	HOOK2	Body	3	4.34E-03	5.28E-03	0.18
chr19:55477653-55477810	158	NLRP2	TSS200, 5'UTR, 1stExon	3	8.58E-03	1.11E-02	-0.06
chr19:15121297-15121385	89	CCDC105	TSS1500, TSS200	3	1.71E-02	2.54E-02	0.06
chr10:134045514-134045609	96	STK32C	Body	3	2.76E-02	2.98E-02	-0.07

Abbreviations: Coord hg19: coordinates of localization in the human genome hg19, starts with the chromosome that contains the genomic region, and the respective rank of differential methylation. Width: the width of the genomic region. Main Gene Assoc: the corresponding principal gene associated with the region according to the used DMRcate's function. Mean p-val: mean of the significant p values corresponding to the probes inside the corresponding genomic range. The p values displayed are the adjusted p values after the Bonferroni correction. Min p-val: the minor of the significant p values corresponding to the probes inside the corresponding genomic range. Mean Dbeta: the net difference between beta values of control group in comparison with AD group.

<sup>a</sup>The names of this genes were annotated and verified by direct visualization in UCSC browser.

terminals when ectopically expressed. In the present study, *BTBD3* was found differently hypermethylated in AD through cg00592643 probe as top result, in addition it was found in the intersection between DMP and DMR analysis (Supplemental Tables 1 and 5). The hypermethylation is located at an island shore in the promoter region of *BTBD3* near to ORegAnno transcription factor binding sites OREG1501119 and OREG1261483 (less than 300 bp).<sup>37</sup> The disruption of *Btbd3* showed an increase in compulsive behavior in mice.<sup>38</sup> Interestingly, differential

methylation of this gene has been associated with obsessive compulsive disorder,<sup>39,40</sup> which has been reported as a risk factor for AD (Figure 3(a)).<sup>41,42</sup>

### *PGPEPIL* (pyroglutamyl-peptidase I like)

*PGPEPIL* gene is responsible to coding Pyroglutamyl-Peptidase 1-Like Protein with putative function of cysteine-type peptidase activity. In this work, *PGPEPIL* was found

**Table 6.** Top results of regions found in the intersection between DMP and DMR analysis.

Seq names	width	gene_assoc	group	#p	Min p	Mean p	"Mean
chr10:34061612-34061705	94			3	7.87E-14	1.86E-13	-0.09
chr6:28984234-28984374	141			6	1.34E-11	2.57E-06	0.07
chr7:92672812-92673176	365			5	3.32E-11	3.99E-06	-0.06
chr20:11870769-11870817	49	BTBD3	TSS1500	2	1.21E-09	1.38E-09	0.07
chr19:52452317-52452528	212			4	6.40E-09	8.75E-05	0.07
chr15:99548859-99549047	189	PGPEP1L <sup>a</sup>	5'UTR, 1stExon, TSS200	4	6.28E-08	9.05E-07	0.06
chr10:76803669-76803925	257	DUSP29 <sup>a</sup> (DUPD1)	Body	3	9.40E-08	1.73E-03	0.06
chr7:64295458-64295583	126			2	3.30E-07	3.31E-07	0.06
chr1:1564920-1565027	108	MIB2	Body	3	5.63E-07	2.86E-05	-0.07
chr6:90597340-90597591	252			4	1.29E-06	5.57E-05	0.06
chr7:5111875-5112067	193	RBAK-RBAKDN <sup>a</sup>	Body	3	1.46E-06	4.29E-04	0.06
chr6:112688010-112688078	69			2	2.92E-05	1.14E-04	0.06
chr14:106661062-106661120	59			2	5.57E-05	1.95E-04	-0.07
chr10:89167457-89167468	12			2	9.65E-05	9.90E-05	0.07
chr1:25944712-25944802	91	MAN1C1	1stExon	2	5.22E-04	8.04E-04	0.07
chr2:233271154-233271185	32	ALPPL2	TSS1500	2	1.81E-03	1.95E-03	-0.08
chr7:27185282-27185393	112	HOXA6	Body	2	4.05E-03	2.27E-02	0.06
chr13:52598798-52598902	105	UTP14C, ALG11	TSS200, Body, 5'UTR, 1stExon	2	1.01E-02	2.10E-02	-0.06

Coord hg19: coordinates of localization in the human genome hg19, starts with the chromosome that contains the genomic region, and the respective rank of differential methylation. Width: the width of the genomic region. Main Gene Assoc: the corresponding principal gene associated with the region according to the used DMRcate's function. Mean p-val: mean of the significant p values corresponding to the probes inside the corresponding genomic range. Only regions with 2 or more CpGs are shown on the table.

<sup>a</sup>The name of this gene was verified by direct visualization in UCSC browser.

**Table 7.** Top results of CpG positions found in the intersection between DMP and DMR.

probeld	Chr	genes	DeltaBeta	t	B	adj. p	dir
cg18931036	chr7	HOXA-AS3, HOXA6	0.10	17.25	76.21	1.36E-32	Hyper
cg05489271	chr12	KMT5A	-0.07	-16.57	72.12	7.97E-31	Hypo
cg04285477	chr14	MIDEAS	-0.13	-16.31	70.48	4.11E-30	Hypo
cg17921863	chr19	BCAM	-0.07	-13.15	50.76	1.55E-21	Hypo
cg12581769	chr19	CACNA1A	0.07	12.62	47.45	4.37E-20	Hyper
cg17809780	chr3	ATG7	-0.10	-11.52	40.48	4.59E-17	Hypo
cg10649706	chr8	AGO2	-0.09	-11.25	38.76	2.58E-16	Hypo
cg13262467	chr3	LRRIQ4	-0.10	-11.02	37.38	1.06E-15	Hypo
cg13815695	chr12	TTC41P	-0.21	-10.79	35.74	5.58E-15	Hypo
cg03464200	chr7	SSPOP	-0.06	-10.58	34.55	1.76E-14	Hypo
cg00700039	chr18	SMCHD1	0.13	10.30	32.81	9.95E-14	Hyper
cg25256924	chr11	CORO1B, PTPRCAP	-0.09	-9.88	30.20	1.38E-12	Hypo
cg00820740	chr10	BICC1	-0.07	-9.87	30.16	1.46E-12	Hypo
cg17086141	chr17	NPEPPS	0.06	9.44	27.58	1.96E-11	Hyper
cg09564509	chr2	HDLBP	-0.09	-8.90	24.28	5.47E-10	Hypo
cg15287806	chr10	ZMYND11	-0.13	-8.42	21.43	9.55E-09	Hypo
cg09529323	chr19	SBK2	-0.08	-8.29	20.72	1.95E-08	Hypo
cg25641145	chr8	ANKRD46	0.10	8.23	20.34	2.86E-08	Hyper
cg24196017	chr15	CDAN1	0.07	8.07	19.40	7.35E-08	Hyper
cg07147421	chr10	FAM245A	0.09	8.06	19.37	7.56E-08	Hyper
cg23047825	chr15	IGF1R	0.07	7.97	18.83	1.32E-07	Hyper
cg14429807	chr9	VAV2	0.06	7.94	18.75	1.51E-07	Hyper
cg23672278	chr1	EVA1B, SH3D21	0.09	7.87	18.29	2.26E-07	Hyper
cg25644478	chr3	LTF	-0.08	-7.51	16.24	1.79E-06	Hypo
cg01697477	chr3	RARB	0.07	7.40	15.66	3.31E-06	Hyper

Probe Id: alphanumeric codes corresponding to the Illumina probe/position; Adj. p: Bonferroni FDR-adjusted p values; B: B-statistic corresponding to the log-odds that the CpG differentially methylated; Chr: chromosome; Dir: direction of differential methylation in AD; Gene symbol: official gene symbol of NIH available in <http://www.ncbi.nlm.nih.gov/gene>; t: value of t-distribution; Δβ: the net difference between beta values of control group and AD group (control—AD).



**Table 8.** Gene ontologies for the differentially methylated genes in Alzheimer's disease in the DMP analysis for InterPro analysis.

Term	Term size	Odds ratio log	Adj. p
Cadherin_N (IPR013164)	69	5.91	4.22E-15
Cadherin (IPR002126)	119	5.31	1.95E-13
Cadherin-like (IPR015919)	131	5.21	2.86E-13
Ig-like_dom (IPR007110)	434	4.09	5.54E-11
SH3_domain (IPR001452)	212	4.39	8.80E-08
PH_domain (IPR001849)	264	4.17	2.73E-07
CD80_C2-set (IPR013162)	57	5.33	1.68E-06
SH3_2 (IPR011511)	181	4.36	1.78E-06
Ig_sub (IPR003599)	384	3.78	1.78E-06
SAM (IPR001660)	90	4.85	5.38E-06
SAM_2 (IPR011510)	84	4.92	5.38E-06
SAM_typeI (IPR021129)	89	4.86	5.38E-06
Ig_V-set (IPR013106)	243	4.06	5.38E-06
Ig_sub2 (IPR003598)	240	4.07	5.38E-06
SAM/pointed (IPR013761)	120	4.55	1.60E-05
PDZ (IPR001478)	148	4.33	3.48E-05
Fibronectin_type3 (IPR003961)	213	3.96	1.32E-04
Ig_L-set (IPR013098)	210	3.97	1.32E-04
Ankyrin_rpt (IPR002110)	235	3.86	1.84E-04
Ankyrin_rpt-contain_dom (IPR020683)	250	3.80	2.23E-04

Term size L: numbers of identifiers annotated in the list of analyzed genes for the term; Odds ratio log: log of odds ratio between the enrichment of the list of the differentially methylated genes in relation to the all genes represented in all the analyzed probes; Adj. p: p value of Fisher's exact test after FDR correction using the Benjamini and Hochberg method; Funt. Term: functional term to gene clustering in enrichment analysis.

differentially hypermethylated in a 189 bp region at exon 1 (5-prime region) in AD compared to controls. The hypermethylated region was located at 59 bp of a TSS of SwitchGear Genomics (code CHR15\_M0654\_R2) considering as a promoter region, therefore related to gene repression. *PGPEPIL* has been related with different types of cancer, with high expression linked to renal cell carcinoma<sup>43</sup> and colorectal cancer progression.<sup>44</sup> In relation with AD, a SNP of *PGPEPIL* (rs35435718) was found to be significant associated. In addition, an epistatic interaction with *NEIL2* in *APOE4*<sup>+</sup> subjects was related to stress response pathway (Figure 3(b)).<sup>45</sup>

### *DUSP29 (dual specificity phosphatase 29, also known as DUPD1)*

This gene encodes for Dual Specificity Phosphatase 29 protein, which dephosphorylates phosphotyrosine, phosphoserine and phosphothreonine residues within the same substrate. A decrease in *DUSP29* expression has been associated with muscle training and cardiorespiratory fitness in rats.<sup>46</sup> Additionally, this gene is upregulated in neurogenic skeletal muscle atrophy.<sup>47</sup> Members of the Dual-Specificity Phosphatases (*DUSP*) are associated with neural

**Table 9.** Gene ontologies for the differentially methylated genes in Alzheimer's disease in the DMP analysis for GO slim.

Functional term	Odds ratio log	p	Adj. p
extracellular matrix organization (GO:0030198)	4.10	1.51E-09	1.22E-07
protein binding transcription factor activity (GO:0000988)	3.40	1.06E-06	4.28E-05
phosphatase activity (GO:0016791)	3.87	2.07E-06	5.58E-05
hydrolase activity, acting on carbon-nitrogen not peptide bonds (GO:0016810)	4.30	1.19E-05	1.60E-04
transcription factor binding (GO:0008134)	3.41	1.26E-05	1.60E-04
mRNA processing (GO:0006397)	3.40	1.27E-05	1.60E-04
ligase activity (GO:0016874)	3.35	1.54E-05	1.60E-04
cell proliferation (GO:0008283)	3.35	1.58E-05	1.60E-04
lipid binding (GO:0008289)	3.09	4.25E-05	3.82E-04
protein targeting (GO:0006605)	3.52	1.16E-04	8.54E-04
translation (GO:0006412)	3.52	1.16E-04	8.54E-04
transferase activity, transferring glycosyl groups (GO:0016757)	3.47	1.32E-04	8.90E-04
cytoplasmic membrane-bounded vesicle (GO:0016023)	3.30	2.21E-04	1.37E-03
chromosome segregation (GO:0007059)	4.31	3.78E-04	2.19E-03
anatomical structure formation involved in morphogenesis (GO:0048646)	3.06	4.41E-04	2.29E-03
translation factor activity, RNA binding (GO:0008135)	4.22	4.51E-04	2.29E-03
neurological system process (GO:0050877)	3.00	5.22E-04	2.45E-03
autophagy (GO:0006914)	4.12	5.43E-04	2.45E-03
plasma membrane organization (GO:0007009)	4.09	5.80E-04	2.47E-03
chromosome (GO:0005694)	3.79	1.03E-03	4.16E-03

Functional term: functional term to gene clustering in enrichment analysis; List positive IDs; odds ratio log: log of odds ratio between the enrichment of the list of the differentially methylated genes in relation to all genes represented in all the analyzed probes; Adj. p: p value of Fisher's exact test after FDR correction using the Benjamini and Hochberg method.

abnormalities.<sup>48</sup> *DUSP29* is expressed in whole blood according the Genotype-Tissue Expression GTEx annotation.<sup>49</sup> In this study, a region of 257 bp was found differentially hypermethylated in AD, in the gene body within intron 1, close to the unique CpG island of this gene.

### *MIB2 (MIB E3 ubiquitin protein ligase 2)*

The *MIB2* gene is a type of Protein Coding gene responsible for encoding an E3 ubiquitin protein ligase. This ligase plays a role in attaching ubiquitin molecules to proteins

**Table 10.** Gene ontologies for the differentially methylated genes in Alzheimer's disease in the DMP analysis for GO biological process.

Term	Term size	Odds ratio log	p	Adj. p
Homophilic cell adhesion via plasma membrane adhesion molecules (GO:0007156)	142	5.12	1.03E-15	1.97E-12
Ossification (GO:0001503)	94	4.80	5.58E-08	3.56E-05
Skeletal system development (GO:0001501)	148	4.33	3.45E-07	1.32E-04
Cell surface receptor signaling pathway (GO:0007166)	205	4.00	1.26E-06	3.23E-04
Notch signaling pathway (GO:0007219)	129	4.17	1.73E-05	1.95E-03
Behavioral response to pain (GO:0048266)	17	5.89	1.88E-05	2.00E-03
regulation of ion transmembrane transport (GO:0034765)	139	4.10	2.16E-05	2.12E-03
Gamma-aminobutyric acid signaling pathway (GO:0007214)	25	5.46	4.14E-05	3.17E-03
Gene silencing by RNA (GO:0031047)	30	5.27E	5.99E-05	3.96E-03
Intracellular signal transduction (GO:0035556)	400	3.02	4.86E-04	2.07E-02
Cell-matrix adhesion (GO:0007160)	92	4.10	5.68E-04	2.27E-02
Cellular response to hypoxia (GO:0071456)	98	4.03	6.44E-04	2.44E-02
positive regulation of cytosolic calcium ion concentration (GO:0007204)	118	3.84	9.30E-04	3.16E-02
Positive regulation of NF-kappa B transcription factor activity (GO:0051092)	122	3.81	9.94E-04	3.23E-02
Negative regulation of cell growth (GO:0030308)	122	3.81	9.94E-04	3.23E-02
regulation of small GTPase mediated signal transduction (GO:0051056)	159	3.54	1.68E-03	4.98E-02

Term size: numbers of identifiers annotated in the list of analyzed genes for the term; odds ratio log: log of odds ratio between the enrichment of the list of the differentially methylated genes in relation to all genes represented in all the analyzed probes; Adj. p: p value of Fisher's exact test after FDR correction using the Benjamini and Hochberg method.

within the Notch signaling pathway, thereby influencing the regulation of Notch1 transcription in microglia. It was found that *MIB2* gene is differentially expressed in brain from AD subjects in circulating leukocytes.<sup>50</sup> *MIB2* highlights several interesting candidate *loci* in which differential DNAm patterns in peripheral tissue are associated with episodic memory performance in humans.<sup>51</sup> It has been suggested to have a critical role in microglial activation and ischemia-induced brain injury in mice.<sup>52</sup> In the present study, *MIB2* was found differently hypomethylated in AD in two neighbor regions inside a 450 CpG island in the 18th exon near 5-prime extreme, in addition it was found in the intersection between DMP and DMR analysis (Tables 1 and 4). The hypomethylation is located at an intronic region near (less than 500 bp) to OregAnno elements evidenced as transcription factor binding sites OREG1487643 and OREG1219540.

### ***FAM234A* (family With sequence similarity 234 member A)**

*FAM234A*, a protein coding gene, was found differentially hypomethylated in this work. The function of *FAM234A* remains unknown; however, diseases associated with *FAM234A* include Filippi Syndrome and Alpha-Thalassemia. In addition, an important paralog of this gene is *FAM234B*, which is associated with neurodevelopmental abnormalities.<sup>53</sup> Interestingly, *FAM234A* has been reported to be up-regulated in Parkinson's disease in the context of *LRKK2* gene carriers.<sup>54</sup> The differentially hypomethylated region of *FAM234A*, spanning 28 bp and located 1308 bp upstream of a transcription start site

(TSS) identified by SwitchGear Genomics (code CHR16\_P0010\_R3), was identified in this study. This finding warrants future exploration of *FAM234A* in AD.

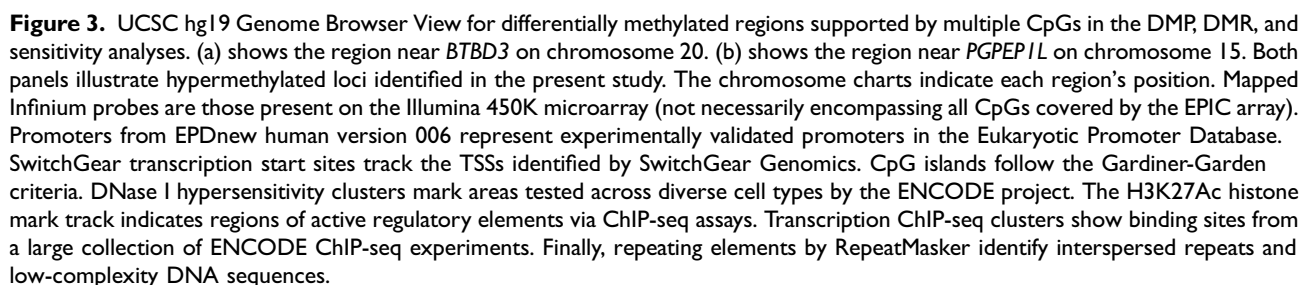
### ***KATNBLIP6* (katanin regulatory subunit B1 like 1 pseudogene 6)**

*KATNBLIP6*, identified as a pseudogene, was found to be differentially hypomethylated in a region spanning 116 bp, with concordance across 6 CpG positions exhibiting the same direction of differential methylation. This finding is challenging to interpret in the context of a pseudogene, but future studies could consider further research.

### ***KMT5A* (lysine methyltransferase 5A)**

The *KMT5A* gene encodes the Lysine N-Methyltransferase 5A Protein, which monomethylate Lys-20 of histone H4, thereby effecting transcriptional repression of certain genes. In the present study, this gene was found differentially hypomethylated. The hypomethylation pattern identified in this study corresponds to the cg05489271 probe, situated 1917 bp from a transcription start site (TSS) of SwitchGear Genomics (code CHR12\_P0857\_R2), and approximately 2 kb from two CpG islands at the 5-prime end of the gene.

*KMT5A*, formerly known as *SET8*, has been implicated in the regulation of multiple biological processes, including gene transcription, the cell cycle, and senescence. This suggests that the loss of *SET8* is sufficient to induce cellular senescence.<sup>55</sup> Intrauterine growth restriction is associated



with low levels of *SET8* and neurodevelopmental disruption.<sup>56</sup> Interestingly, literature reports that ENST00000537270, an isoform of *KMT5A*, has been associated with an increased risk of schizophrenia in GWAS studies.<sup>57</sup> To the author's knowledge, this represents the first report of *KMT5A/SET8* involvement in AD.

### ***MIDEAS (mitotic deacetylase associated SANT domain protein)***

*MIDEAS* is implicated in histone deacetylation and negative regulation of transcription.<sup>58</sup> In this study, it was found to be differentially hypomethylated at the cg04285477 position, located 1363 bp from a transcription start site (TSS) of SwitchGear Genomics (code CHR14\_M0378\_R5). A prior study indicated that *DNTTIP1* and *MIDEAS* regulate a highly similar set of target genes in different contexts, and their MiDAC complex controls a neurodevelopmental gene expression program; this program includes genes crucial for guiding neurite growth and morphogenesis.<sup>59</sup>

### ***BCAM (basal cell adhesion molecule)***

The *BCAM* gene, located on chromosome 19 near *APOE*, encodes a basal cell adhesion glycoprotein expressed in blood and other tissues. It regulates cell migration through interactions with other adhesion molecules.<sup>60</sup> In the present study, *BCAM* was identified as differentially hypomethylated at a CpG site in both DMR and DMP analyses (Tables 3 and 6). The position cg17921863 is located 2342 bp from CHR19\_P0676\_R2 and on a CpG island shelf. Interestingly, genetic variations in *BCAM* have been found to be strongly associated with A $\beta$ <sub>1-42</sub> concentrations in the cerebrospinal fluid of AD patients.<sup>61</sup>

### ***HOXA-AS3 (HOXA cluster antisense RNA 3) and HOXA6 (homeobox A6)***

The current study identified the position cg18931036 as differentially hypermethylated in AD compared to controls; this position corresponds to *HOXA-AS3* and *HOXA6* genes. Furthermore, cg18931036 is located within a CpG island common to both genes. This position is situated at 1388 bp of a TSS corresponding of *HOXA-AS3* (code CHR7\_P0179\_R2). *HOXA-AS3* is an RNA gene associated with the long non-coding RNA (lncRNA) class. Its expression has been correlated with cancer, including glioblastoma. Furthermore, *HOXA-AS3* is involved in regulating biological processes such as cell proliferation, invasion, and migration.<sup>62</sup> Interestingly, *HOXA-AS3* was found to be differentially hypermethylated in cerebral cortex in previous studies in AD.<sup>63</sup> On the other hand, the cg18931036

position is located approximately 2000 pb from a TSS corresponding to *HOXA6* (code CHR7\_M0173\_R1). *HOXA6* gene encodes Homeobox A6 Protein, a DNA-binding transcription factor with a clear regulatory function. Interestingly, in previous studies in prefrontal cortex and superior frontal gyrus, a region encompassing *HOXA3* to *HOXA6* genes was found differentially methylated in AD.<sup>35,64</sup> Interestingly, *HOXA-AS3* was found to be differentially hypermethylated in cerebral cortex in previous studies in AD.<sup>63</sup> On the other hand, the cg18931036 position is located approximately 2000 pb from a TSS corresponding to *HOXA6* (code CHR7\_M0173\_R1). *HOXA6* gene encodes Homeobox A6 Protein, a DNA-binding transcription factor with a clear regulatory function. Interestingly, in previous studies in prefrontal cortex and superior frontal gyrus, a region encompassing *HOXA3* to *HOXA6* genes was found differentially methylated in AD.<sup>35,64</sup>

### ***CACNA1A (calcium voltage-gated channel subunit Alpha 1 A)***

*CACNA1A* encodes voltage-sensitive calcium channels (VSCC) that mediate the entry of calcium ions into excitable cells. The current study identified a CpG position (cg12581769) differentially hypermethylated in AD, situated 2869 bp from a CpG island within the *CACNA1A* gene body. *CACNA1A* has been associated with ataxia and other neurologic disorders,<sup>65</sup> including the motor disruption observed in AD among human PS1-E280A carriers and APPsw/PS1 $\Delta$ 9 mice.<sup>66,67</sup>

### ***PCDHGB1-3 (protocadherin gamma subfamily B, 1 to 3) and PCDHGA1-6 (protocadherin gamma subfamily A, 1 to 6)***

The surrogate genes found differentially methylated in the current study were *PCDHGB1-3* and *PCDHGA1-6*. According to UniProt, a repository of protein sequences and annotations, all these genes may play a role in the establishment and maintenance of specific neuronal connections in the brain.<sup>68</sup> Changes in DNA methylation of protocadherins have been associated with various human diseases, including schizophrenia and responses to their treatment.<sup>69</sup> Interestingly, *PCDHGB1* was found differentially hypomethylated in cerebellar cortex in AD.<sup>70</sup> Detection of protocadherin methylation changes in blood, using surrogate CpGs derived from brain data, reinforces the concept that specific peripheral epigenetic alterations mirror central nervous system epigenetic changes in Alzheimer's disease. This concordance between blood and cerebellum supports the potential of these surrogate CpGs as candidate biomarkers.

On the other hand, gene enrichment analysis indicated a clear relationship between immune process with epigenetic disrupted in AD, in addition to molecular processes of intracellular signaling. The results could be related to AD systemic inflammatory disruption and neuroplasticity affection detectable in blood as a surrogate of brain tissue.

A recent whole-genome methylation sequencing study in blood by Madrid et al. (2025) examined MCI and AD subjects and reported DNA methylation changes associated with cognitive status. That study identified 9756 DMPs and 1743 differentially methylated genes.<sup>71</sup> Our findings showed only limited gene-level overlap with those results, with a few individual genes identified in both studies (e.g., the autophagy-related gene *ATG7* and several protocadherin-alpha family genes involved in cell adhesion). Nevertheless, both our array-based study and the sequencing study by Madrid et al. converged on similar biological themes. In particular, both analyses revealed differential methylation in genes linked to immune/inflammatory processes, synaptic function (including neurotransmission and synapse organization), and neurodevelopmental pathways (such as those governing dendritic structure and neuronal plasticity). This alignment in functional categories suggests that, despite distinct cohorts and platforms, blood DNA methylation changes in AD consistently implicate pathways related to inflammation, synaptic integrity, and neurodevelopment.

The current study showed partial concordance with other previous report on the gene *HOXB6*;<sup>72</sup> the cg01324550 probe with a delta beta of approximately 0.05, was found with no exact genomic concordance (nominal p-value <0.05). Another study, focusing on late-onset mild cognitive impairment, reported 11 significant genes validated through gene expression analysis. Among them, two genes were found to be differentially expressed in the current study with an exact genomic match. The *ZNF415* gene on the cg05769153 probe was identified as differentially hypermethylated, with a delta beta of approximately 7% (nominal p-value 0.0055556). Similarly, *SNED1* exhibited partial concordance across three CpGs; cg22635676 was found to be concordantly differentially hypomethylated, whereas cg15361291 and cg21384492 were discordantly hypermethylated compared to a previous report of hypomethylation (nominal p < 0.05; delta beta approximately 5%).<sup>73</sup>

Variability in sample handling and storage is inherent in public database studies. Our quality control, using a detection p-value filter and ComBat batch correction, reduces technical variability so that differential methylation more closely reflects underlying biology.

This study has several limitations. The AD group was significantly older than the control group; although age was adjusted for in all analyses, residual effects may persist, suggesting that future research would benefit from age-matched cohorts and longitudinal designs. The analysis relied on secondary public data with limited clinical

information (e.g., *APOE* genotype, disease duration, and co-morbid conditions), and the cohorts comprised primarily patients with later-stage AD, which may enhance detection of differential methylation but limit generalizability to early-stage cases. Technical variations between the GEO datasets, including differences in array processing, were addressed with rigorous normalization and batch correction using BMIQ and ComBat; however, some variability may remain. Moreover, the Infinium 450K array interrogates only a limited portion of the human methylome, and is inherently limited compared to the comprehensiveness of whole-genome methylation sequencing.<sup>71</sup> The lack of available SNP genotype data prevented an integrative meQTL analysis to evaluate the influence of genetic risk variants on methylation. Finally, the cross-sectional design and absence of an independent replication cohort limit causal inference. While these findings are consistent with previous reports of differential methylation in AD blood samples,<sup>27</sup> ongoing validation in additional samples is required to establish their clinical and biological significance as candidate biomarkers.

The present study contributes with possible biomarkers that can be the basis for research on non-invasive diagnostic methods in AD. The identification of altered epigenetic patterns would allow future studies to focus on strategies to modify cellular genetic regulation in personalized medicine.


## Conclusions


This study identified DNA methylation patterns in peripheral blood leukocytes that may serve as potential biomarkers for AD. The profile found includes genes related to immune responses and dendritic field orientation. While these findings offer preliminary insights into epigenetic changes related to systemic inflammation in AD, they are hypothesis-generating and require further validation in longitudinal studies with additional clinical and multi-modal data.

## Acknowledgments

The authors have no acknowledgments to report.

## ORCID iDs

Tatiana Chacón  <https://orcid.org/0000-0001-8712-3123>

Hernán G Hernández  <https://orcid.org/0000-0001-8479-6269>

## Ethical considerations

The original studies secured appropriate informed consent and ethical approvals.<sup>26–28</sup>

## Consent to participate

The original studies secured appropriate informed consent and ethical approvals.<sup>26–28</sup>

## Consent for publication

Not applicable.

## Author contributions

Tatiana Chacon (Conceptualization; Data curation; Formal analysis; Investigation; Methodology; Validation; Writing – original draft; Writing – review & editing); Hernan Guillermo Hernandez (Conceptualization; Formal analysis; Project administration; Supervision; Validation; Writing – original draft; Writing – review & editing)

## Funding

The authors disclosed receipt of the following financial support for the research, authorship, and/or publication of this article: This project was funded by FODEIN grant award from Universidad Santo Tomás – Colombia.

## Declaration of conflicting interests

The authors declared no potential conflicts of interest with respect to the research, authorship, and/or publication of this article.

## Data availability

Data used in this study was available in Gene Expression Omnibus data set GSE59685 and GSE53740 (available at <https://www.ncbi.nlm.nih.gov/geo/>).

## Supplemental material

Supplemental material for this article is available online.

## References

- Castellani RJ, Rolston RK and Smith MA. Alzheimer disease. *Dis Mon* 2010; 56: 484–546.
- Kumar A, Singh A and Ekavali E. A review on Alzheimer's disease pathophysiology and its management: an update. *Pharmacol Rep* 2015; 67: 195–203.
- Remarque EJ, Bollen EL, Weverling-Rijnsburger AW, et al. Patients with Alzheimer's disease display a pro-inflammatory phenotype. *Exp Gerontol* 2001; 36: 171–176.
- Park JC, Han SH and Mook-Jung I. Peripheral inflammatory biomarkers in Alzheimer's disease: a brief review. *BMB Rep* 2020; 53: 10–19.
- Angiulli F, Conti E, Zoia CP, et al. Blood-based biomarkers of neuroinflammation in Alzheimer's disease: a central role for periphery? *Diagnostics (Basel)* 2021; 11: 1525.
- Li QS, Vasanthakumar A, Davis JW, et al. Association of peripheral blood DNA methylation level with Alzheimer's disease progression. *Clin Epigenetics* 2021; 13: 191.
- d'Abramo C, D'Adamio L and Giliberto L. Significance of blood and cerebrospinal fluid biomarkers for Alzheimer's disease: sensitivity, specificity and potential for clinical use. *J Pers Med* 2020; 10: 116.
- Teunissen CE, Verberk IMW, Thijssen EH, et al. Blood-based biomarkers for Alzheimer's disease: towards clinical implementation. *Lancet Neurol* 2022; 21: 66–77.
- Weinberg DN, Papillon-Cavanagh S, Chen H, et al. The histone mark H3K36me2 recruits DNMT3A and shapes the intergenic DNA methylation landscape. *Nature* 2019; 573: 281–286.
- Fransquet PD, Lacaze P, Saffery R, et al. Blood DNA methylation as a potential biomarker of dementia: a systematic review. *Alzheimers Dement* 2018; 14: 81–103.
- Henderson AR, Wang Q, Meechoovet B, et al. DNA Methylation and expression profiles of whole blood in Parkinson's disease. *Front Genet* 2021; 12: 640266.
- Gerring ZF, Lupton MK, Edey D, et al. An analysis of genetically regulated gene expression across multiple tissues implicates novel gene candidates in Alzheimer's disease. *Alzheimers Res Ther* 2020; 12: 43.
- Mendonca V, Soares-Lima SC and Moreira MAM. Exploring cross-tissue DNA methylation patterns: blood-brain CpGs as potential neurodegenerative disease biomarkers. *Commun Biol* 2024; 7: 904.
- Silva TC, Young JI, Zhang L, et al. Cross-tissue analysis of blood and brain epigenome-wide association studies in Alzheimer's disease. *Nat Commun* 2022; 13: 4852.
- Peng X, Zhang W, Cui W, et al. ADmeth: a manually curated database for the differential methylation in Alzheimer's disease. *IEEE/ACM Trans Comput Biol Bioinform* 2023; 20: 843–851.
- Braun PR, Han S, Hing B, et al. Genome-wide DNA methylation comparison between live human brain and peripheral tissues within individuals. *Transl Psychiatry* 2019; 9: 47.
- Tsalamandris S, Antonopoulos AS, Oikonomou E, et al. The role of inflammation in diabetes: current concepts and future perspectives. *Eur Cardiol* 2019; 14: 50–59.
- Calsolaro V and Edison P. Neuroinflammation in Alzheimer's disease: current evidence and future directions. *Alzheimers Dement* 2016; 12: 719–732.
- Hu WT, Holtzman DM, Fagan AM, et al. Plasma multianalyte profiling in mild cognitive impairment and Alzheimer disease. *Neurology* 2012; 79: 897–905.
- Pillai JA, Bena J, Bebek G, et al. Inflammatory pathway analytes predicting rapid cognitive decline in MCI stage of Alzheimer's disease. *Ann Clin Transl Neurol* 2020; 7: 1225–1239.
- Liew CC, Ma J, Tang HC, et al. The peripheral blood transcriptome dynamically reflects system wide biology: a potential diagnostic tool. *J Lab Clin Med* 2006; 147: 126–132.
- Stylianou E. Epigenetics of chronic inflammatory diseases. *J Inflamm Res* 2019; 12: 1–14.
- Wang AL, Qiu W, DeMeo DL, et al. DNA Methylation is associated with improvement in lung function on inhaled corticosteroids in pediatric asthmatics. *Pharmacogenet Genomics* 2019; 29: 65–68.
- Zimmer-Bensch G and Zempel H. DNA Methylation in genetic and sporadic forms of neurodegeneration: lessons from Alzheimer's, related tauopathies and genetic tauopathies. *Cells* 2021; 10: 3064.



25. Liu X, Jiao B and Shen L. The epigenetics of Alzheimer's disease: factors and therapeutic implications. *Front Genet* 2018; 9: 579.
26. Lunnon K, Smith R, Hannon E, et al. Methylomic profiling implicates cortical deregulation of ANK1 in Alzheimer's disease. *Nat Neurosci* 2014; 17: 1164–1170.
27. Hannon E, Lunnon K, Schalkwyk L, et al. Interindividual methylomic variation across blood, cortex, and cerebellum: implications for epigenetic studies of neurological and neuropsychiatric phenotypes. *Epigenetics* 2015; 10: 1024–1032.
28. Li Y, Chen JA, Sears RL, et al. An epigenetic signature in peripheral blood associated with the haplotype on 17q21.31, a risk factor for neurodegenerative tauopathy. *PLoS Genet* 2014; 10: e1004211.
29. Clough E and Barrett T. The gene expression omnibus database. *Methods Mol Biol* 2016; 1418: 93–110.
30. Davis S and Meltzer PS. GEOquery: a bridge between the gene expression omnibus (GEO) and BioConductor. *Bioinformatics* 2007; 23: 1846–1847.
31. Hernández HG, Hernández-Castañeda AA, Pieschacón MP, et al. ZNF718, HOXA4, and ZFP57 are differentially methylated in periodontitis in comparison with periodontal health: epigenome-wide DNA methylation pilot study. *J Periodontol Res* 2021; 56: 710–725.
32. Teschendorff AE, Marabita F, Lechner M, et al. A beta-mixture quantile normalization method for correcting probe design bias in illumina infinium 450 k DNA methylation data. *Bioinformatics* 2013; 29: 189–196.
33. Hop PJ, Zwamborn RAJ, Hannon EJ, et al. Cross-reactive probes on Illumina DNA methylation arrays: a large study on ALS shows that a cautionary approach is warranted in interpreting epigenome-wide association studies. *NAR Genom Bioinform* 2020; 2: lqaa105.
34. Lehne B, Drong AW, Loh M, et al. A coherent approach for analysis of the Illumina HumanMethylation450 BeadChip improves data quality and performance in epigenome-wide association studies. *Genome Biol* 2015; 16: 37.
35. Hernández HG, Sandoval-Hernández AG, Garrido-Gil P, et al. Alzheimer's disease DNA methylome of pyramidal layers in frontal cortex: laser-assisted microdissection study. *Epigenomics* 2018; 10: 1365–1382.
36. Hung JH, Yang TH, Hu Z, et al. Gene set enrichment analysis: performance evaluation and usage guidelines. *Brief Bioinform* 2012; 13: 281–291.
37. Montgomery SB, Griffith OL, Sleumer MC, et al. OReganno: an open access database and curation system for literature-derived promoters, transcription factor binding sites and regulatory variation. *Bioinformatics* 2006; 22: 637–640.
38. Thompson SL, Welch AC, Ho EV, et al. Btd3 expression regulates compulsive-like and exploratory behaviors in mice. *Transl Psychiatry* 2019; 9: 222.
39. Stewart SE, Yu D, Scharf JM, et al. Genome-wide association study of obsessive-compulsive disorder. *Mol Psychiatry* 2013; 18: 788–798.
40. Yue W, Cheng W, Liu Z, et al. Genome-wide DNA methylation analysis in obsessive-compulsive disorder patients. *Sci Rep* 2016; 6: 31333.
41. Ruggeri M, Ricci M, Gerace C, et al. Late-onset obsessive-compulsive disorder as the initial manifestation of possible behavioural variant Alzheimer's disease. *Cogn Neuropsychiatry* 2022; 27: 11–19.
42. Chen MH, Cheng CM, Tsai SJ, et al. Obsessive-compulsive disorder and dementia risk: a nationwide longitudinal study. *J Clin Psychiatry* 2021; 82: 20m13644.
43. Wang P, Chen J, Ye X, et al. Circ-PGPEP1 augments renal cell carcinoma proliferation, Warburg effect, and distant metastasis. *Acta Biochim Pol* 2023; 70: 703–711.
44. Zhang C, Zhang C, Liu X, et al. Circular RNA PGPEP1 induces colorectal cancer malignancy and immune escape. *Cell Cycle* 2023; 22: 1743–1758.
45. Dato S, De Rango F, Crocco P, et al. Sex- and APOE-specific genetic risk factors for late-onset Alzheimer's disease: evidence from gene-gene interaction of longevity-related loci. *Aging Cell* 2023; 22: e13938.
46. Sadler DG, Treas L, Ross T, et al. Parental cardiorespiratory fitness influences early life energetics and metabolic health. *Physiol Genomics* 2024; 56: 145–157.
47. West R and Waddell D. Dual specificity phosphatase and pro isomerase domain containing 1 (Dupd1) is upregulated during neurogenic skeletal muscle atrophy and is differentially expressed in MuRF1-null mice. *FASEB J* 2017; 31 (Supp 1): 1021.10–1021.10.
48. Bhore N, Wang BJ, Chen YW, et al. Critical roles of dual-specificity phosphatases in neuronal proteostasis and neurological diseases. *Int J Mol Sci* 2017; 18: 1963.
49. Consortium GT. The GTEx consortium atlas of genetic regulatory effects across human tissues. *Science* 2020; 369: 1318–1330.
50. Bahado-Singh RO, Vishweswaraiah S, Aydas B, et al. Artificial intelligence and leukocyte epigenomics: evaluation and prediction of late-onset Alzheimer's disease. *PLoS One* 2021; 16: e0248375.
51. Sommerer Y, Dobricic V, Schilling M, et al. Epigenome-wide association study in peripheral tissues highlights DNA methylation profiles associated with episodic memory performance in humans. *Biomedicine* 2022; 10: 2798.
52. Li X, Liao Y, Dong Y, et al. Mib2 deficiency inhibits microglial activation and alleviates ischemia-induced brain injury. *Aging Dis* 2020; 11: 523–535.
53. Poulton C, Baynam G, Yates C, et al. A review of structural brain abnormalities in Pallister-Killian syndrome. *Mol Genet Genomic Med* 2018; 6: 92–98.
54. Karayel O, Virreira Winter S, Padmanabhan S, et al. Proteome profiling of cerebrospinal fluid reveals biomarker candidates for Parkinson's disease. *Cell Rep Med* 2022; 3: 100661.
55. Fukuura K, Inoue Y, Miyajima C, et al. The ubiquitin-specific protease USP17 prevents cellular senescence by

- stabilizing the methyltransferase SET8 and transcriptionally repressing p21. *J Biol Chem* 2019; 294: 16429–16439.
56. Milite C, Feoli A, Viviano M, et al. The emerging role of lysine methyltransferase SETD8 in human diseases. *Clin Epigenetics* 2016; 8: 102.
  57. Mahoney R, Bendl J, Kozlenkov A, et al. F93. Cell-type specific transcriptomic profiling in schizophrenia identifies changes in gabaergic neurons and oligodendrocytes at transcript level. *Eur Neuropsychopharmacol* 2023; 75: S270.
  58. Itoh T, Fairall L, Muskett FW, et al. Structural and functional characterization of a cell cycle associated HDAC1/2 complex reveals the structural basis for complex assembly and nucleosome targeting. *Nucleic Acids Res* 2015; 43: 2033–2044.
  59. Mondal B, Jin H, Kallappagoudar S, et al. The histone deacetylase complex MiDAC regulates a neurodevelopmental gene expression program to control neurite outgrowth. *Elife* 2020; 9: e57519.
  60. Liu M, Liao L, Gao Y, et al. BCAM Deficiency may contribute to preeclampsia by suppressing the PIK3R6/p-STAT3 signaling. *Hypertension* 2022; 79: 2830–2842.
  61. Nho K, Kim S, Horgusluoglu E, et al. Association analysis of rare variants near the APOE region with CSF and neuroimaging biomarkers of Alzheimer's disease. *BMC Med Genomics* 2017; 10: 29.
  62. Yao Q, Wang C, Wang Y, et al. The integrated comprehension of lncRNA HOXA-AS3 implication on human diseases. *Clin Transl Oncol* 2022; 24: 2342–2350.
  63. Li QS, Sun Y and Wang T. Epigenome-wide association study of Alzheimer's disease replicates 22 differentially methylated positions and 30 differentially methylated regions. *Clin Epigenet* 2020; 12: 149.
  64. Smith RG, Hannon E, De Jager PL, et al. Elevated DNA methylation across a 48-kb region spanning the HOXA gene cluster is associated with Alzheimer's disease neuropathology. *Alzheimers Dement* 2018; 14: 1580–1588.
  65. Andrade A, Brennecke A, Mallat S, et al. Genetic associations between voltage-gated calcium channels and psychiatric disorders. *Int J Mol Sci* 2019; 20: 3537.
  66. Kang S, Gim J, Lee J, et al. Potential novel genes for late-onset Alzheimer's disease in East-Asian descent identified by APOE-stratified genome-wide association study. *J Alzheimers Dis* 2021; 82: 1451–1460.
  67. Sepulveda-Falla D, Barrera-Ocampo A, Hagel C, et al. Familial Alzheimer's disease-associated presenilin-1 alters cerebellar activity and calcium homeostasis. *J Clin Invest* 2014; 124: 1552–1567.
  68. UniProt C. Uniprot: a hub for protein information. *Nucleic Acids Res* 2015; 43: D204–D212.
  69. El Hajj N, Dittrich M and Haaf T. Epigenetic dysregulation of protocadherins in human disease. *Semin Cell Dev Biol* 2017; 69: 172–182.
  70. Semick SA, Bharadwaj RA, Collado-Torres L, et al. Integrated DNA methylation and gene expression profiling across multiple brain regions implicate novel genes in Alzheimer's disease. *Acta Neuropathol* 2019; 137: 557–569.
  71. Madrid A, Papale LA, Bergmann PE, et al. Whole genome methylation sequencing in blood from persons with mild cognitive impairment and dementia due to Alzheimer's disease identifies cognitive status. *Alzheimers Dement* 2025; 21: e14474.
  72. Roubroeks JAY, Smith AR, Smith RG, et al. An epigenome-wide association study of Alzheimer's disease blood highlights robust DNA hypermethylation in the HOXB6 gene. *Neurobiol Aging* 2020; 95: 26–45.
  73. Zhang Y and Shen S. Epigenome-wide DNA methylation analysis of late-stage mild cognitive impairment. *Front Cell Dev Biol* 2024; 12: 1276288.